

Origin of spin-glass-like magnetic anomaly in the superconducting and multiferroic spin ladder BaFe_2Se_3

W. G. Zheng ¹, V. Balédent,¹ L. Bocher,¹ A. Forget,² D. Colson,² and P. Foury-Leylekian ^{1,*}

¹*Université Paris-Saclay, CNRS, Laboratoire de Physique des Solides, 91405, Orsay, France*

²*SPEC, CEA, CNRS-UMR3680, Université Paris-Saclay, Gif-sur-Yvette Cedex 91191, France*



(Received 3 October 2022; revised 16 December 2022; accepted 12 January 2023; published 26 January 2023)

The spin ladder system BaFe_2Se_3 presents puzzling magnetic behaviors, such as a spin-glass-like phase below ~ 50 K. In this paper, an exchange bias effect with a large vertical shift in the field-cooled hysteresis loop is observed below 50 K. We also evidence the existence of uncompensated spins by susceptibility, magnetic remanence, and hysteresis loop measurements. The thermoremanent and isothermoremanent magnetization curves evidence a two-dimensional diluted antiferromagnet (DAFF) nature. Moreover, a nanometer-sized layered structure is observed by scanning electron microscope (SEM) and confirmed by scanning transmission electron microscope (STEM) coupled with electron energy loss spectroscopy (EELS). The discovery of exchange bias in antiferromagnetic BaFe_2Se_3 crystals adds a new dimension to the research of its superconducting and multiferroic properties.

DOI: [10.1103/PhysRevB.107.024423](https://doi.org/10.1103/PhysRevB.107.024423)

I. INTRODUCTION

During the last decade, the quasi-one-dimensional compound BaFe_2Se_3 attracted a lot of attention because of its multiferroic property and superconductivity [1,2]. The superconducting phase emerges between 10 and 15 GPa below 11 K [2]. A ferroelectric state is also evidenced and persists up to ~ 600 K [3]. The Fe atoms form a ladder structure. Each ladder is constituted of two Fe legs, which extend along the b axis [4]. BaFe_2Se_3 exhibits an unconventional block antiferromagnetic order below the Néel temperature (T_N) [5]. The Fe moments of about $3 \mu_B$ are parallel or anti-parallel to the a axis, which is also the magnetic easy axis [6]. Besides, puzzling magnetic features are reported at low temperature: (i) An anomaly in the susceptibility curve below a frozenlike temperature $T_f \sim 50$ K and (ii) the absence of long-range magnetic transition at T_f in the neutron diffraction measurements [5,7,8]. Until now, this behavior has been attributed to a spin-glass transition coming from either the underlying magnetic frustration or the presence of random spins [6,7,9]. In this work, we propose a microscopic interpretation of the T_f anomaly in terms of the exchange bias effect.

The exchange bias effect was discovered by Meiklejohn and Bean in Co particles covered with antiferromagnetic oxide CoO [10]. Generally, the exchange bias (EB) is characterized by a horizontal shift of the magnetic hysteresis loop after field-cooling (FC). It occurs in various systems, which possess interfaces between antiferromagnetic (AFM) and ferromagnetic (FM) phases, like AFM/FM thin film bilayers, nanoparticles, AFM single crystal coated with an FM material, and even spin glasses [11]. On the microscopic scale, uncompensated spins of the AFM phase which are coupled

to the FM phase by magnetic exchanges are believed to be at the origin of the exchange bias effect [12,13]. Moreover, the presence of a vertical shift of the magnetic hysteresis loop under FC is observed in a few systems: Bilayers or multilayers of AFM and FM [12,14–19], nanoparticles with AFM core and FM shell [20–23] or ferrimagnetic (FIM) core and AFM shell [24]. In the systems above, interfaces between at least two different AFM and FM/FIM materials are required. Although it is relatively rare, an exchange bias with vertical shift can also be observed in some antiferromagnetic systems without the presence of ferromagnetism, e.g., on NiO, $\text{BiFe}_{0.8}\text{Mn}_{0.2}\text{O}_3$, or maghemite nanoparticles [25–27], Co_3O_4 nanowires [28], and Co-doped ZnO films [29]. In these cases, the EB effect is attributed to uncompensated spins related either to uncompensated AFM sublattices in a nanoparticle or to dilute AFM in a field (DAFF) in a core-shell system such as Co_3O_4 [28]. Despite the large variety of EB systems, the presence of uncompensated or disordered spins is always the key to understanding the microscopic mechanism of the exchange bias effect [11,29].

In this paper, we focus on the complex magnetic properties of BaFe_2Se_3 at low temperature. We investigate the spin-glass-like transition by studying the hysteresis loops in zero-field-cooling (ZFC) and field-cooling (FC). By thermoremanent magnetization (TRM) and isothermoremanent magnetization (IRM) curves, we evidence that the sizable exchange bias effect is related to a 2D-DAFF behavior instead of a classical spin glass. We finally demonstrate that the intrinsic layered structure of the BaFe_2Se_3 single crystals is responsible for an exchange bias effect.

II. EXPERIMENTAL

High-quality single-crystal BaFe_2Se_3 were grown by the melt-growth method [6]. We first mixed the small pieces of

*Corresponding author: pascale.foury@u-psud.fr

Ba (99.9%), powder of Fe (99.9%), and Se (99.999%) with the nominal composition 1:2:3. The resulting pellets were placed in a carbon crucible and then sealed in an evacuated quartz tube with a partial pressure of 300 mbar of Ar gas. The quartz tube is then annealed and cooled to obtain the crystal. Magnetic properties were measured by a commercial superconducting quantum interference device (SQUID) on various magnetic fields and temperatures. The scanning electron microscopy (SEM) images were recorded using a Zeiss Supra 55 VP SEM (Zeiss, Oberkochen, Germany). To further assess the atomic and elemental structures of the BaFe_2Se_3 single crystals down to the atomic scale, we additionally acquire high-angle annular dark-field (HAADF) images in a C3/C5-corrected Nion UltraSTEM 200 operated at 100 kV with 30 mrad convergence angle, 50 mrad EELS collection angle, and around 50 pA of probe current. The microscope is equipped with a Medipix3 direct electron detection (Merlin EM Quantum Detectors). EELS spectra were gain-corrected with a gain reference acquired prior to the experiments. Spectrum-images were denoised using Principal Component Analyses retaining the first four components. Cross-sectional electron-transparent samples were prepared for electron spectro-microscopy (STEM-EELS) studies by focused ion-beam on a SCIOS dual-beam platform (FEI-Thermofischer) following the standard procedure.

III. RESULTS

A. Magnetometry

The quality of the BaFe_2Se_3 crystals used for our magnetic measurements has been checked by single-crystal diffraction and powder neutron diffraction in our previous paper [30]. The temperature dependence of dc magnetization under 10 kOe has been measured along a (perpendicular to the ladder plane), b (leg), and c (rung) directions, respectively [Fig. 1(a)]. The decrease below T_N (around 200 K) along the a axis indicates the presence of long-range AFM order as reported in Ref. [30]. Besides, the increasing of the b and c magnetic components with cooling shows that the antiferromagnetic easy axis is along the a -axis. Below $T_f \sim 50$ K, the ZFC and FC (under 10 kOe) curves, mainly along a and c , move away from each other while it is not the case along b . This behavior has also been reported in Refs. [6,7,31] as well as in Ref. [8] for Co-doped BaFe_2Se_3 system. The origin was attributed to a spin-glass effect [7,31].

We thus checked a spin-glass origin for this behavior. As shown in Fig. 1(b), we applied 10 kOe at room temperature and cooled the sample down to 5 K, then switch off the external field and measured the remanent magnetization. An immediate drop was observed, incompatible with a spin glass state that would relax slowly [inset of Fig. 1(b)]. This observation challenged the spin-glass nature of BaFe_2Se_3 .

We then measured the magnetization as a function of the magnetic field at low temperature after ZFC and FC from 300 K. As shown in Fig. 2(a), the ZFC curve shows a hysteresis, with a coercivity of $H_C = 325 \pm 15$ Oe, unusual for an antiferromagnetic bulk material. Besides, we also observed that the magnetization does not saturate up to 70 kOe (not shown). This indicates that the field cannot easily align the

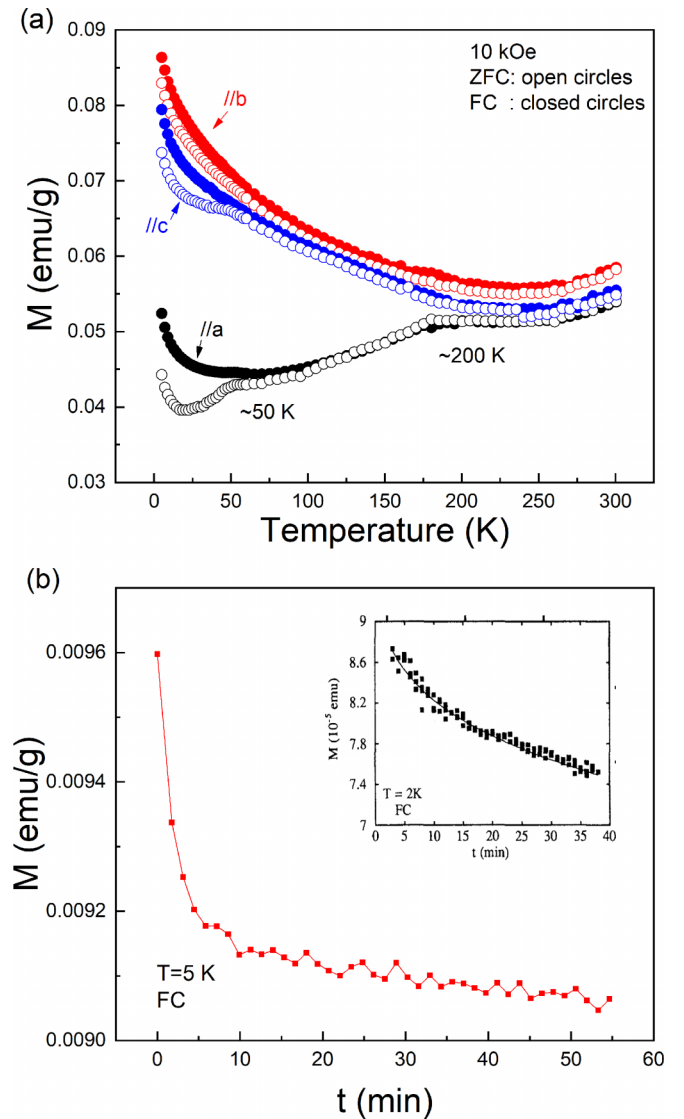


FIG. 1. (a) Temperature dependence of dc magnetization for BaFe_2Se_3 . The magnetic field of 10 kOe is applied along the a , b , and c axes. The open and close circles represent the curves after ZFC and FC, respectively. (b) Time dependence of the remanent magnetization measured immediately after the field setting to zero. The inset shows the case of $\text{La}_{1.96}\text{Sr}_{0.04}\text{CuO}_4$ which displays a spin-glass behavior below 7 K [32].

magnetic domains and the exchange interactions J_{AFM} are strong which is consistent with the high T_N ($200 \text{ K} = 17 \text{ meV} = 1000 \text{ kOe}$ for $2.8 \mu_B$ Fe moments as determined experimentally [30]). The FM-like cycle could be due to (i) a small amount of ferromagnetic impurities (ii) interfacial or trapped uncompensated spins [12,18,22,25,28,29,33]. As for the FC curves measured after cooling with applied fields of ± 10 kOe, they show similar trends: A hysteresis loop, a similar coercivity within the error bars, and unsaturated magnetization at 70 kOe. In addition, the FC curves exhibit a remarkable vertical shift (M_{shift}) in the direction depending on the sign of the cooling field. M_{shift} is defined as $[(M_{\text{max}} + M_{\text{min}})/2]/[(M_{\text{max}} - M_{\text{min}})/2]$ [33], where M_{max} and M_{min} are the maximum and minimum of the hysteresis loop. No

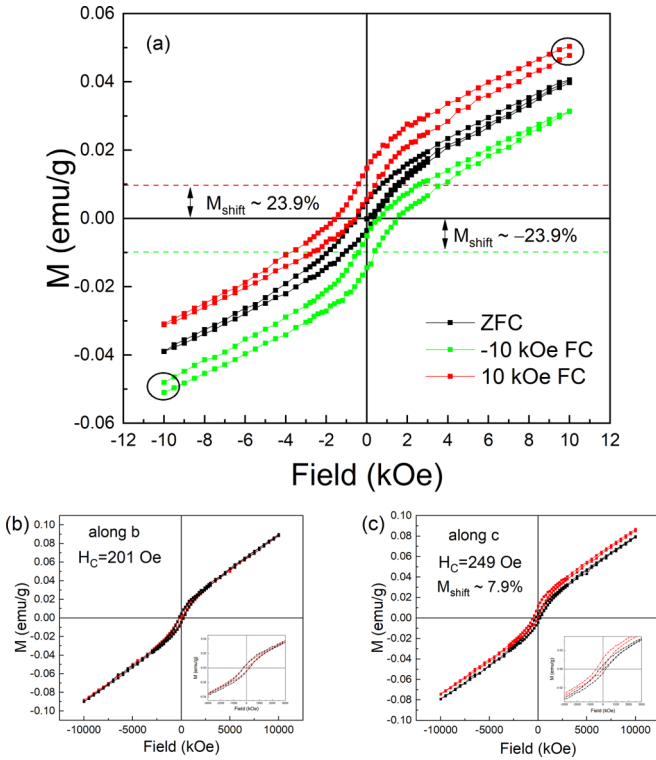


FIG. 2. (a) Hysteresis loops for the applying field along a at 5 K after ZFC and FC. [(b) and (c)] Hysteresis loops for the applying field along b and c , respectively. The cooling field is 10 kOe for the FC measurement.

obvious horizontal shift was observed. Besides, the FC curves display a loop opening, emphasized by the black circles in Fig. 2(a), which could be the fingerprint of uncompensated spins in the sample [18,29]. Interestingly, as shown in Fig. 2, while the hysteresis behavior is present whatever the direction of the applied magnetic field, the vertical shift is only visible for H along a or c , similar to the bifurcations in the temperature dependence of magnetization measurements in Fig. 1(a). The coercivities of the FC curves are 201 ± 10 and 249 ± 10 Oe for H along b and c , respectively. This not only suggests that the two features have different origin but also reveals an anisotropy of M_{shift} .

To further understand the possible origin of this unusual behavior at 50 K, we performed TRM and IRM measurements [28]. TRM is the remanent magnetization in zero field after FC while for IRM the field is applied after ZFC and then cut off to measure the remanent magnetization in zero field [see the inset of Fig. 3(a)]. Usually, for a spin glass, the TRM curve displays a peak at low field, and the IRM curve meets the TRM one at high field [28]. As can be seen in Fig. 3(a), the TRM for BaFe_2Se_3 increases continuously with increasing field while the IRM stays low even at high field. Such a behavior is characteristic of a diluted AFM in a field (DAFF) [28]. A power law fit of the TRM curve as a function of H , derived from random field Ising model [28,34], gives an exponent of $\nu_H = 0.63$ [Fig. 3(a)]. For bulk DAFF systems, this exponent is generally found to be close to $\nu_H = 3$ [35]. Our small value for ν_H is rather consistent with a 2D finite-size DAFF system [28].

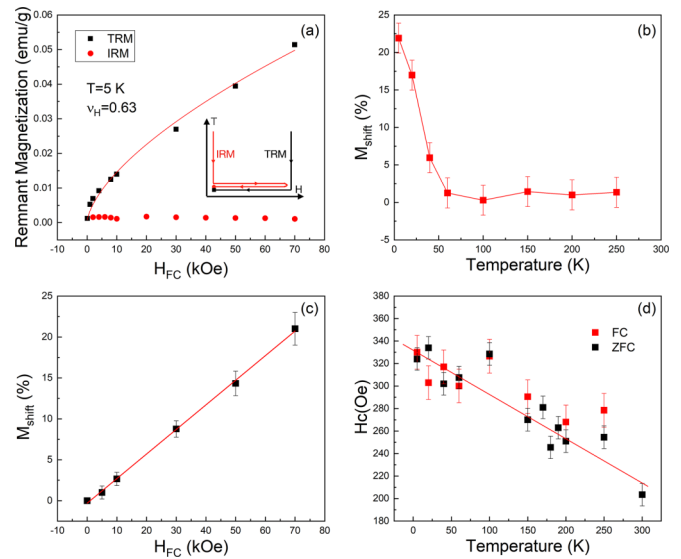


FIG. 3. (a) TRM and IRM vs H_{FC} of BaFe_2Se_3 at 5 K. The red line is the fitting to the power law, $\text{TRM} \propto H^{\nu_H}$. The inset shows how the field changed with temperature during the measurement of TRM and IRM. (b) Temperature dependence of the vertical shift after FC. (c) The vertical shift as a function of cooling field H_{FC} at 5 K. The red line is a linear fitting of the data. (d) Temperature dependence of coercivity in the hysteresis loops after ZFC and FC, respectively. The data is from the same measurements of (b). The red line is a guide for the eyes.

We then studied the temperature dependence of M_{shift} for FC curves. All hysteresis loops are recorded between ± 10 kOe at different temperatures after cooling from 300 K under a field of 10 kOe. As shown in Fig. 3(b), the M_{shift} vanishes above 50 K, suggesting an intricate link with the $T_f \sim 50$ K anomaly observed in the magnetization measurements. This result behaves as the bifurcation between FC and ZFC curves which starts to increase below T_f in Fig. 1(a). Indeed, this M_{shift} is non zero only in the temperature range where ZFC and FC curves differ from each other. The interpretation of this result in term of DAFF-like behavior enables to give an order of magnitude for the magnetic coupling between uncompensated spins: $J_{\text{DAFF}} = k_B T_f = 4.2$ meV. The corresponding magnetic field for the $2.8 \mu_B$ Fe ordered moments determined experimentally [30], would be around 250 kOe. Above 250 kOe, a saturation of the magnetization due to spin flip is expected. To test this interpretation, we studied the evolution of M_{shift} as a function of the FC magnetic field at 5 K. The hysteresis loop was measured between ± 70 kOe after cooling down to 5 K under H_{FC} with different H_{FC} values from 0 to 70 kOe. As reported in Fig. 3(c), M_{shift} increases linearly with H_{FC} , showing no sign of saturation up to 70 kOe. The same behavior was found previously in some nanosystems [19,36].

As for the temperature dependence of coercive fields (H_c), presented in Fig. 3(d), no significant difference between ZFC and FC is observed. The thermal variation of H_c displays a monotonic decrease with increasing temperature but remains finite ($H_c = 200 \pm 15$ Oe) at 300 K. The absence of anomalies at specific temperatures

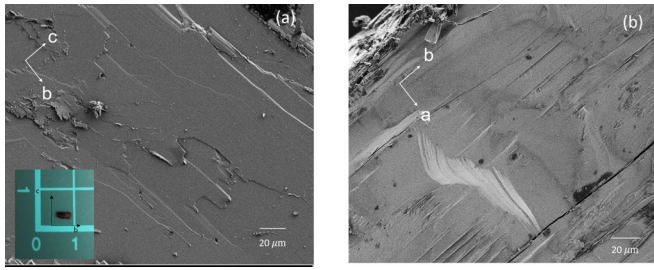


FIG. 4. [(a) and (b)] SEM images of bc and ab planes, respectively.

T_f and T_N keeps the interpretation of FM-like hysteresis elusive.

B. Electron microscopy measurements

These results, pointing toward an effect of 2D-DAFF, seem to be irreconcilable with the fact that our measurements are done on single crystals. Indeed, in a bulk system, surface defects cannot produce such a strong exchange bias signal. To resolve the inconsistency, we performed SEM measurements on the BaFe_2Se_3 crystal. A piece of $0.5 \times 2 \times 5 \text{ mm}^3$ was used [inset of Fig. 4(a)]. The largest face of the crystal is related to the bc plane [9]. Figures 4(a) and 4(b) show the bc and ab surfaces of the crystal, respectively. Many cleavages can be observed on the ab plane, while it is flatter on the bc plane.

Furthermore, to study the nature of the cleavages, we extracted a cross-sectional FIB lamella to perform the STEM/EELS studies along the c axis. A typical low-magnification HAADF-STEM image of the BaFe_2Se_3 crystal on the ab plane is presented in Fig. 5(a). Interestingly, nanometer-thick planar faults with a darker contrast in HAADF mode can be well-identified among the BaFe_2Se_3 lattice, i.e., characterized by a brighter HAADF contrast. All these planar faults are aligned parallel to the b axis. At higher magnification in Fig. 5(b), atomic planes can be clearly distinguished in these darker planar faults, ruling out amorphous regions. This change in HAADF contrast in the planar faults may originate from different reasons since the HAADF intensity is roughly proportional to the Z^2 , the crystallographic density as well as the probed thickness. In Fig. 5(c), the atomically resolved HAADF-STEM image of the BaFe_2Se_3 lattice confirms the expected atomic structure [see inset Fig. 5(c)] where the darker contrasts correspond to the lines of Fe columns, while the brighter ones to the Ba/Se atomic columns forming a zig-zag chain with an intermediate HAADF contrast assigned for the single Ba columns. To clarify the elemental structure of the planar faults, core-loss hyper-spectral data were acquired in the region of interest [marked by a red rectangle in Fig. 5(d)] across a 3.5-nm-thick planar fault by probing both Fe- $L_{2,3}$ and Ba- $M_{4,5}$ edges. Figures 5(e) and 5(f) present the reconstructed Ba- M_5 and Fe- L_3 maps, respectively, on the top and bottom well crystallized regions as well as in the layered fault. Figures 5(h) and 5(g) represent the combined Ba- M_5 (in cyan) and Fe- L_3 (in red) maps and the relative Ba and Fe profiles, respectively, for the same region of interest. In top and bottom well crystallized regions, the elemental structure between Ba and Fe planes

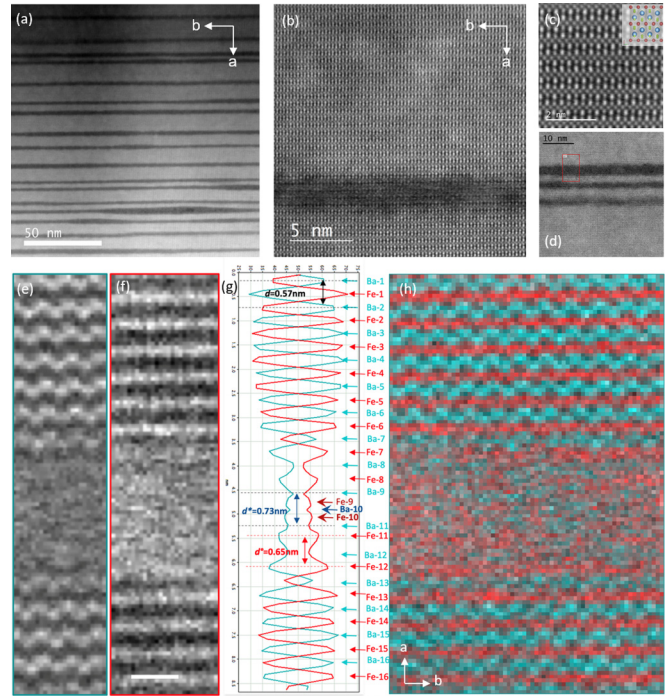


FIG. 5. (a) Low-magnification HAADF-STEM image of the BaFe_2Se_3 crystal along the a - b plane. (b) High-magnification HAADF-STEM image presenting a typical planar fault. (c) Atomically resolved HAADF-STEM image of the BaFe_2Se_3 structure supported with an atomic model for guiding the reader. The red, green, and blue balls represent Fe, Se, and Ba, respectively. (d) HAADF-STEM image including the region of interest, i.e., highlighted by the red rectangle, where the EELS hyper-spectral acquisition was performed across a nanometer-scale planar fault. [(e) and (f)] Elemental reconstructed maps from Ba- M_5 and Fe- L_3 edges, respectively, probed across the planar fault and (h) the corresponding “false” color map combining both Ba (red) and Fe (cyan) components. (g) Relative Ba and Fe composition profiles extracted from the map (h) and summed along the b direction, parallel to the planar fault.

is well retrieved as expected for the BaFe_2Se_3 lattice characterized by a typical interdistance d between atomic planes as depicted in Fig. 5(g). In the planar fault, both Fe and Ba profiles present lower intensities, i.e., from Ba-7 to Ba-13 line in Fig. 5(g), however atomic planes can be still distinguished confirming the ordered nature of these planar faults. One should note that in average the relative Ba intensity remains always below 0.5 while the Fe one is higher than 0.5 indicating a likely Ba deficiency in the planar fault. At both top and bottom interfaces between the BaFe_2Se_3 lattice/planar fault, the termination planes correspond both to the Fe planes, i.e., Fe-6 and Fe-13 lines. Interestingly, an additional Ba plane, i.e., Ba-10, is clearly determined in the middle of the planar fault yielding a structural accommodation along the a axis. Indeed, interdistances (Ba-9 to -11) and (Fe-11 to -12) increase up to 0.73 nm compared to the nominal interdistance $d = 0.57$ nm in the BaFe_2Se_3 lattice. Hence, a single additional Ba plane along the a axis and the subsequent structural accommodation over few nm on both sides of this extra plane yields to such nm-thick planar fault feature running along the a axis. In addition, a slight deficiency of Ba is probed on average in the planar fault.

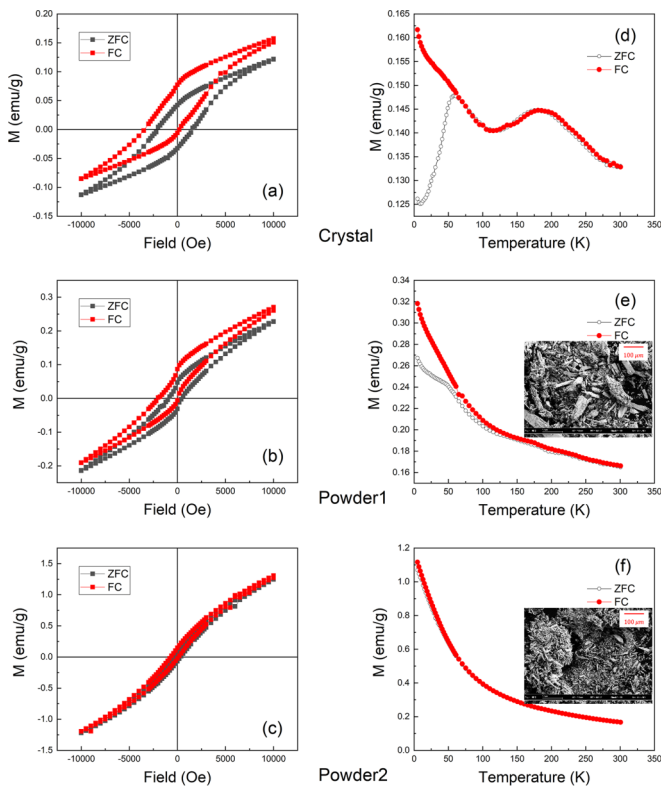


FIG. 6. [(a)–(c)] ZFC and FC hysteresis loops of crystal (along a), powder1, and powder2 measured at 5 K. [(d)–(f)] Temperature dependence of ZFC and FC magnetization curves under 10 kOe for crystal (along a), powder1, and powder2. The insets of (e) and (f) show the SEM images of powder1 and powder2, respectively.

To further investigate the influence of this layered morphology on the magnetic properties, we ground the crystal in two successive steps to obtain two different grain sizes. The average grain lengths estimated from our SEM images were 75 and 35 μm , that we refer in the following as powder1 and powder2, respectively. The SEM images of the two powder samples are shown in the insets of Figs. 6(e) and 6(f). Notice that the grains present a needle-like shape. As reported in Figs. 6(a)–6(c), the hysteresis loop amplitude decreases by reducing the grain size. As any ferromagnetic impurity would have not been affected by grinding, this hypothesis can be ruled out. The grain size reduction also affects the M_{shift} which is almost absent for powder2 [see Figs. 6(d)–6(f)]. These observations are compatible with the 2D-DAFF nature of the sample which is destroyed by the grinding. Indeed, the grinding is likely to affect mainly the regions with weak mechanical properties. We can thus infer from our results that the grinding preferentially targets the stacking faults. The interfaces associated with the 2D-DAFF are ruined, and the hysteresis loop and M_{shift} disappear.

IV. DISCUSSION

Based on our results, we propose a phenomenological model to explain the 50 K anomaly of magnetic susceptibility

characterized by the bifurcation between the FC and ZFC curves as well as the vertical shift of the magnetization upon field cooling. Let us recall that the BaFe_2Se_3 single crystals are in fact made of stacks along the a -axis of ordered layers and planar faults. In the ordered layers, the spins S_{AFM} are in a block AFM state associated with strong exchange interactions J_{AFM} as T_N is high. The S_{AFM} spins can only be aligned under a strong magnetic field and are thus expected to behave similarly in our FC or ZFC measurements. As for the thin planar faults, they are responsible for the 2D-DAFF behavior characterized by a bifurcation between the FC and ZFC curves and a specific evolution of the TRM and IRM curves as a function of H_{FC} [28]. The spins in the 2D-DAFF appear to be coupled by J_{DAFF} which is reduced compared to J_{AFM} . A vertical shift of the global magnetization after FC is also expected to be due to these AFM-DAFF multilayers such as in core-shell systems [28]. This M_{shift} should naturally disappear at T_f , as observed. Therefore, the vertical shift in our single crystal with a layered structure can originate from additional effects due to the multiple interfaces which give rise to the surface or trapped uncompensated spins.

As for the FM-like cycle, we also attribute this effect to surface/interface uncompensated spins which could present FM behavior. Indeed, the magnetic structure is made of blocks of four FM Fe spins ordered in an AFM manner along the ladder. Thus islands of FM uncompensated spins can appear at the interfaces and lead to a FM cycle. Another contribution to the FM behavior usually comes from free uncompensated spins as well as disordered spins in the 2D-DAFF layers because they behave as free moments. When grinding the crystals, the number of interfaces between ordered layers and planar faults is reduced. Thus the FM character and the M_{shift} amplitude disappear.

In conclusion, we elucidated in this paper the origin of the 50 K anomaly of magnetization measurement in BaFe_2Se_3 attributing it to a 2D-DAFF. We also evidenced that our crystals, which present the same quality as the ones of the previous literature (a good mosaicity and a 200 K AFM transition and multiferroic behaviors [30]), are in fact layered structures. This particular morphology leads to an exchange bias effect which adds a new interest in the investigation of the superconducting and multiferroic character of this Fe spin ladder.

ACKNOWLEDGMENTS

This work was financially supported by the ANR COCOM 20-CE30-0029 and the CSC scholarship (No. 201806830111). We acknowledge the Physical Measurements Platform (for magnetometry measurements) and MORPHEUS platform (for crystals alignment) of Laboratoire de Physique des Solides, Université Paris-Saclay. In particular, we thank P. Senzier and H. Raffy for their help during the AC measurements. We also acknowledge the funding from the French National Research Agency under the “Investissements d’Avenir” program TEMPOS (No. ANR-10-EQPX-50) for FIB access.

- [1] S. Dong, J. M. Liu, and E. Dagotto, *Phys. Rev. Lett.* **113**, 187204 (2014).
- [2] J. Ying, H. Lei, C. Petrovic, Y. Xiao, and V. V. Struzhkin, *Phys. Rev. B* **95**, 241109(R) (2017).
- [3] K. Du, L. Guo, J. Peng, X. Chen, Z.-N. Zhou, Y. Zhang, T. Zheng, Y.-P. Liang, J.-P. Lu, Z.-H. Ni, S.-S. Wang, G. V. Tendeloo, Z. Zhang, S. Dong, and H. Tian, *npj Quantum Mater.* **5**, 49 (2020).
- [4] H. Hong and H. Steinfink, *J. Solid State Chem.* **5**, 93 (1972).
- [5] J. M. Caron, J. R. Neilson, D. C. Miller, A. Llobet, and T. M. McQueen, *Phys. Rev. B* **84**, 180409(R) (2011).
- [6] H. Lei, H. Ryu, A. I. Frenkel, and C. Petrovic, *Phys. Rev. B* **84**, 214511 (2011).
- [7] Y. Nambu, K. Ohgushi, S. Suzuki, F. Du, M. Avdeev, Y. Uwatoko, K. Munakata, H. Fukazawa, S. Chi, Y. Ueda, and T. J. Sato, *Phys. Rev. B* **85**, 064413 (2012).
- [8] F. Du, Y. Hirata, K. Matsubayashi, Y. Uwatoko, Y. Ueda, and K. Ohgushi, *Phys. Rev. B* **90**, 085143 (2014).
- [9] X. Liu, C. Ma, C. Hou, Q. Chen, R. Sinclair, H. Zhou, Y. Yin, and X. Li, *Europhys. Lett.* **126**, 27005 (2019).
- [10] W. H. Meiklejohn and C. P. Bean, *Phys. Rev.* **102**, 1413 (1956).
- [11] J. Nogués and I. K. Schuller, *J. Magn. Magn. Mater.* **192**, 203 (1999).
- [12] H. Ohldag, A. Scholl, F. Nolting, E. Arenholz, S. Maat, A. T. Young, M. Carey, and J. Stö, *Phys. Rev. Lett.* **91**, 017203 (2003).
- [13] M. Kiwi, *J. Magn. Magn. Mater.* **234**, 584 (2001).
- [14] J. Nogués, C. Leighton, and I. K. Schuller, *Phys. Rev. B* **61**, 1315 (2000).
- [15] Z. Y. Liu, *Appl. Phys. Lett.* **85**, 4971 (2004).
- [16] H. Ohldag, H. Shi, E. Arenholz, J. Stöhr, and D. Lederman, *Phys. Rev. Lett.* **96**, 027203 (2006).
- [17] M. Gruyters and D. Schmitz, *Phys. Rev. Lett.* **100**, 077205 (2008).
- [18] R. Rana, P. Pandey, and D. S. Rana, *Appl. Phys. Lett.* **104**, 092413 (2014).
- [19] S. J. Yuan, L. Li, T. F. Qi, L. E. DeLong, and G. Cao, *Phys. Rev. B* **88**, 024413 (2013).
- [20] A. N. Dobrynin, D. N. Ievlev, K. Temst, P. Lievens, J. Margueritat, J. Gonzalo, C. N. Afonso, S. Q. Zhou, A. Vantomme, E. Piscopiello, and G. Van Tendeloo, *Appl. Phys. Lett.* **87**, 012501 (2005).
- [21] X. Sun, N. Frey Huls, A. Sigdel, and S. Sun, *Nano Lett.* **12**, 246 (2012).
- [22] E. Passamani, C. Larica, C. Marques, A. Takeuchi, J. Proveti, and E. Favre-Nicolin, *J. Magn. Magn. Mater.* **314**, 21 (2007).
- [23] G. Salazar-Alvarez, J. Sort, S. Suriñach, M. D. Baró, and J. Nogués, *J. Am. Chem. Soc.* **129**, 9102 (2007).
- [24] Z. M. Tian, S. L. Yuan, S. Y. Yin, L. Liu, J. H. He, H. N. Duan, P. Li, and C. H. Wang, *Appl. Phys. Lett.* **93**, 222505 (2008).
- [25] R. H. Kodama, S. A. Makhlof, and A. E. Berkowitz, *Phys. Rev. Lett.* **79**, 1393 (1997).
- [26] P. K. Manna, S. M. Yusuf, R. Shukla, and A. K. Tyagi, *Phys. Rev. B* **83**, 184412 (2011).
- [27] H. Khurshid, W. Li, M.-H. Phan, P. Mukherjee, G. C. Hadjipanayis, and H. Srikanth, *Appl. Phys. Lett.* **101**, 022403 (2012).
- [28] M. J. Benitez, O. Petravic, E. L. Salabas, F. Radu, H. Tüysüz, F. Schüth, and H. Zabel, *Phys. Rev. Lett.* **101**, 097206 (2008).
- [29] B. Henne, V. Ney, M. de Souza, and A. Ney, *Phys. Rev. B* **93**, 144406 (2016).
- [30] W. Zheng, V. Balédent, M. B. Lepetit, P. Retailleau, E. V. Elslande, C. R. Pasquier, P. Auban-Senzier, A. Forget, D. Colson, and P. Foury-Leylekian, *Phys. Rev. B* **101**, 020101(R) (2020).
- [31] B. Saparov, S. Calder, B. Sipo, H. Cao, S. Chi, D. J. Singh, A. D. Christianson, M. D. Lumsden, and A. S. Sefat, *Phys. Rev. B* **84**, 245132 (2011).
- [32] F. C. Chou, N. R. Belk, M. A. Kastner, R. J. Birgeneau, and A. Aharony, *Phys. Rev. Lett.* **75**, 2204 (1995).
- [33] M. Zheng, X. Li, W. Xiao, W. Wang, and H. Ni, *Appl. Phys. Lett.* **111**, 152405 (2017).
- [34] J. Villain, *Phys. Rev. Lett.* **52**, 1543 (1984).
- [35] F. C. Montenegro, S. M. Rezende, and M. D. Coutinho-Filho, *Rev. Bras. Fis.* **21**, 192 (1991).
- [36] M. Buchner, B. Henne, V. Ney, and A. Ney, *Phys. Rev. B* **99**, 064409 (2019).